Supplementary Information

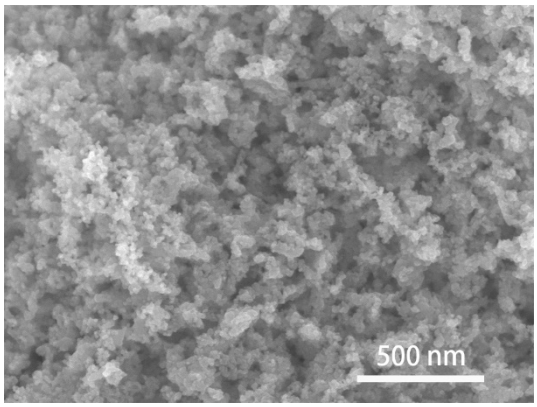

Figure S1. SEM image of $Ru_{0.9}Cr_{0.1}O_2$.

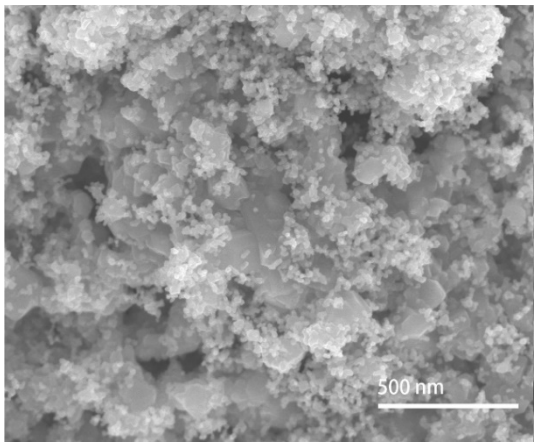

Figure S2. SEM image of RuO_2.

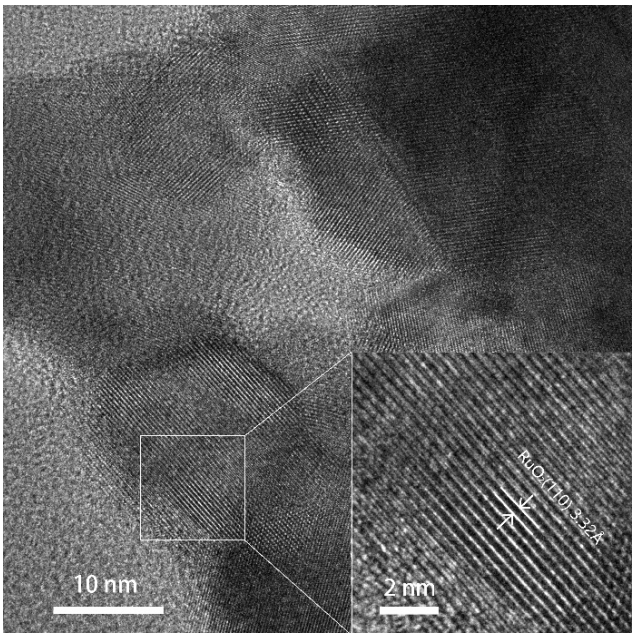

Figure S3. HRTEM images of RuO_2.

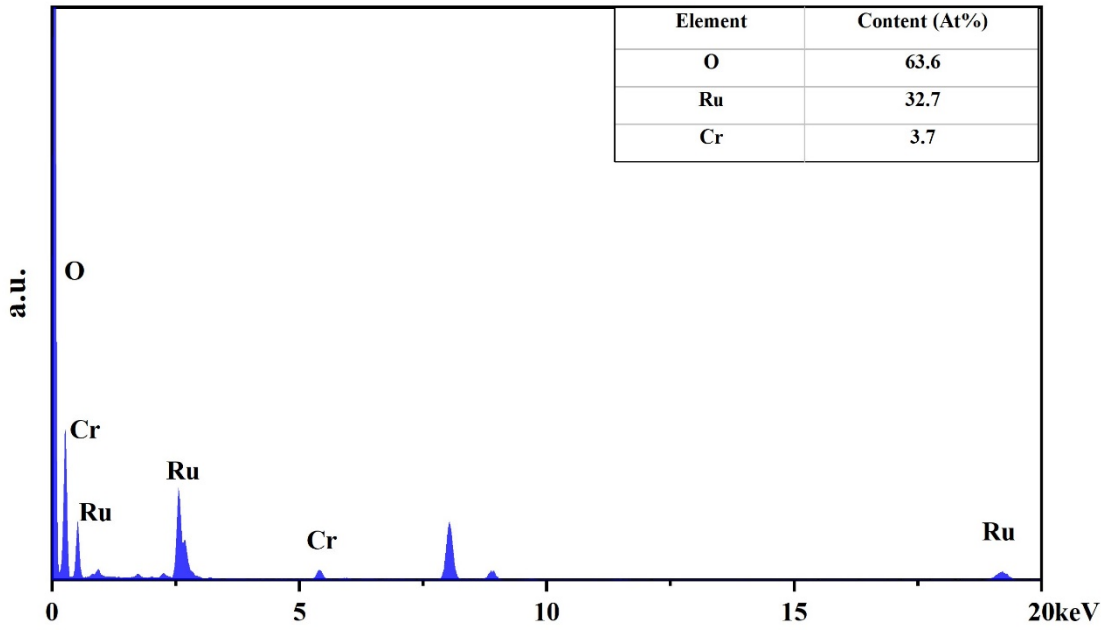

Figure S4. EDS elemental spectra of $Ru_{0.9}Cr_{0.1}O_2$.

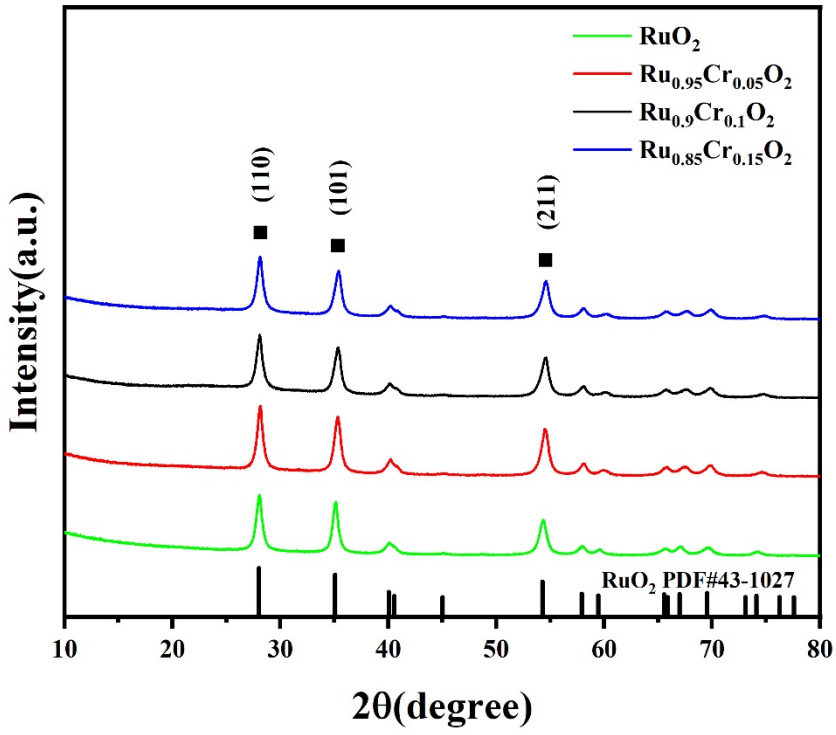

Figure S5. XRD of unmodified and different Cr-doped RuO_2.

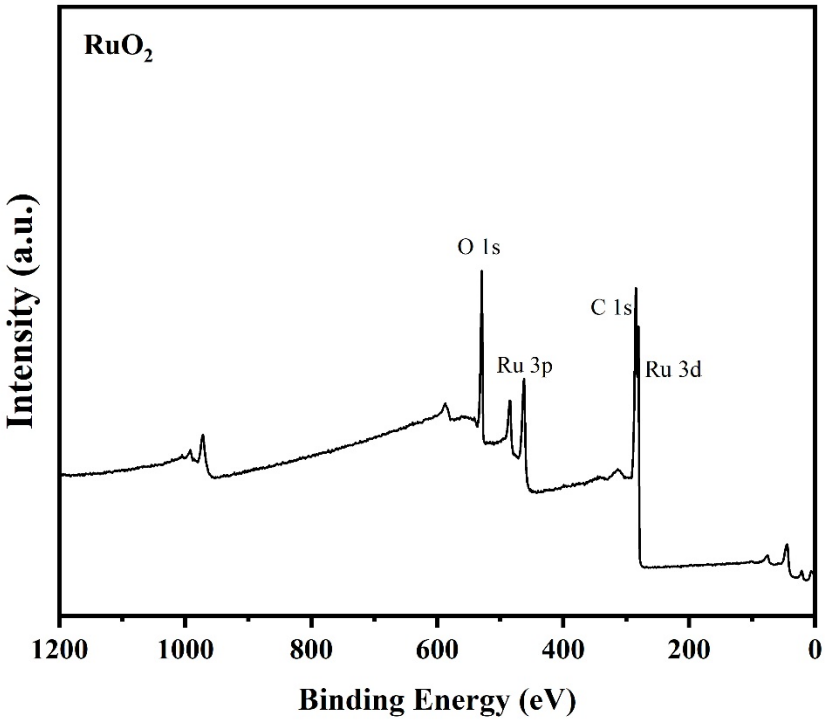

Figure S6. XPS survey pattern of RuO_2.

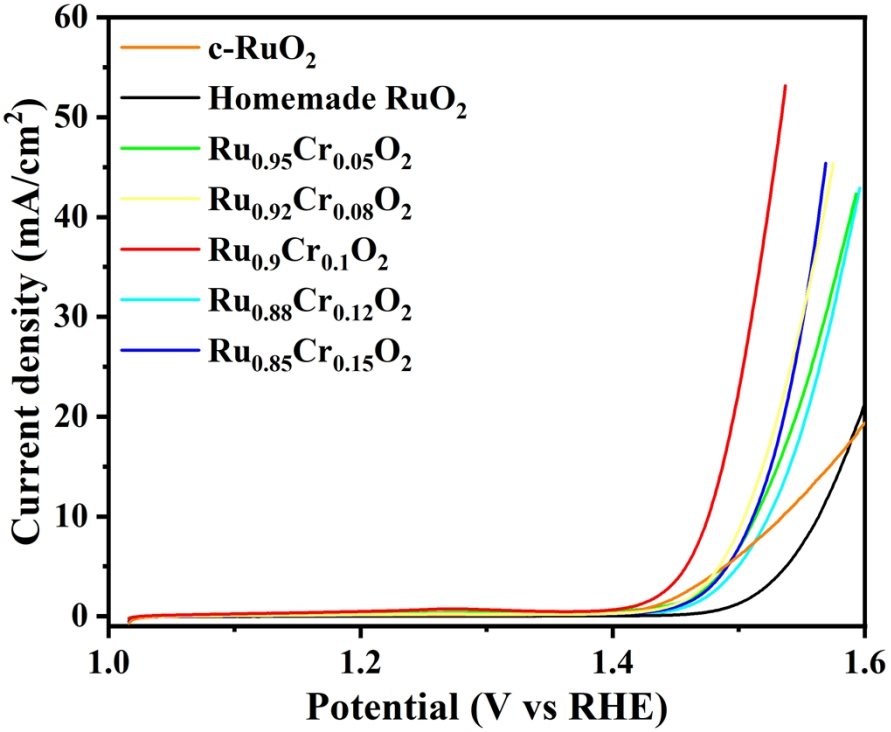

Figure S7. LSV curves of RuO_2 with different Cr-doped.

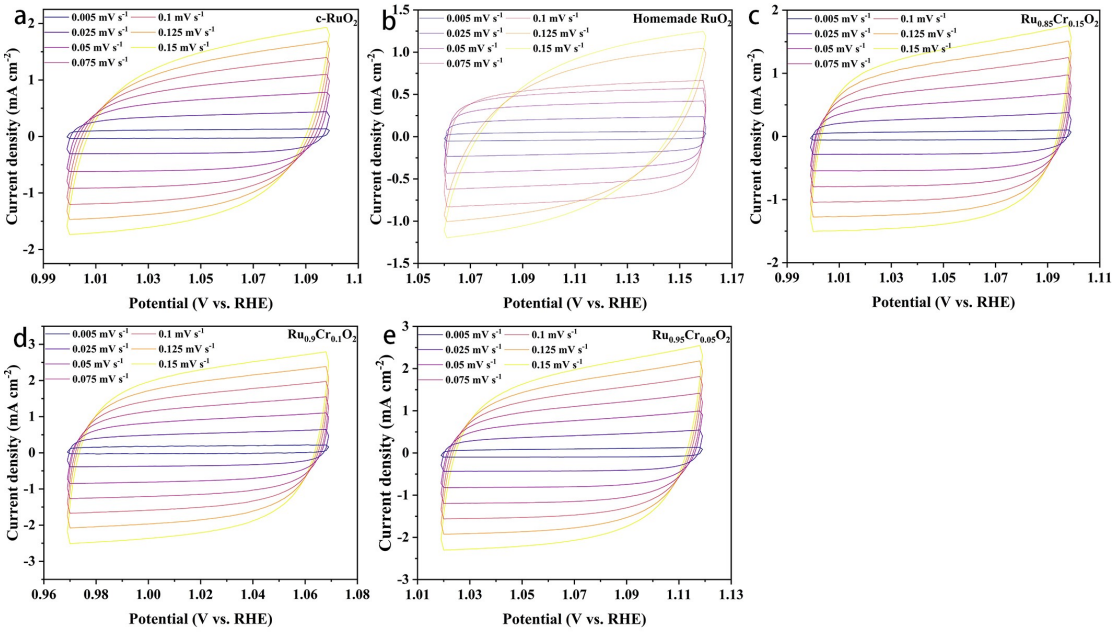

Figure S8. CV curves of (a) c-RuO_2, (b) homemade RuO_2, (c) $Ru_{0.9}Cr_{0.1}O_2$, (d) $Ru_{0.9}Cr_{0.1}O_2$ and (e) $Ru_{0.9}Cr_{0.1}O_2$ in the non-Faradaic region under different scan rates in pH=0 H_2SO_4.

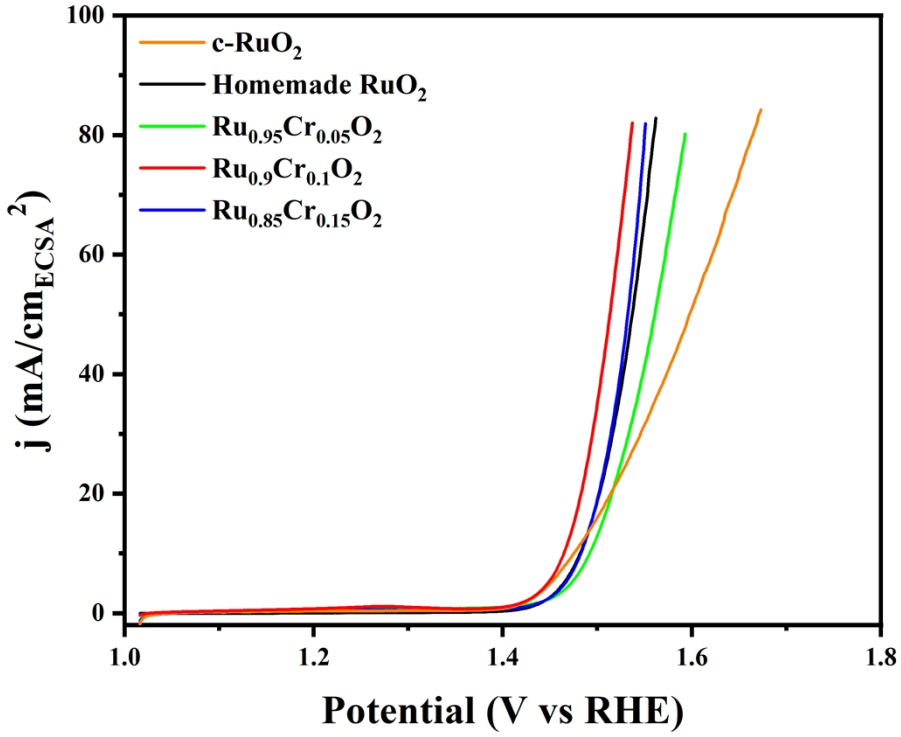

Figure S9. LSV curves after ECSA normalization.

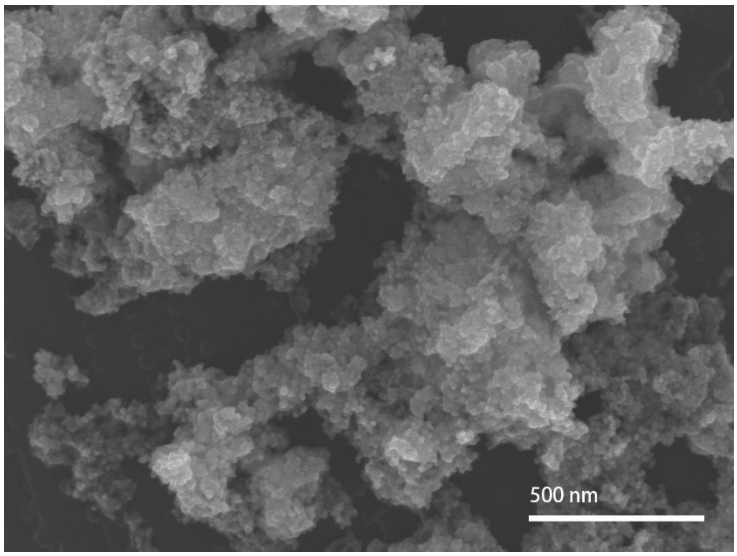

Figure S10. SEM image of $Ru_{0.9}Cr_{0.1}O_2$ after 8 h CP test.

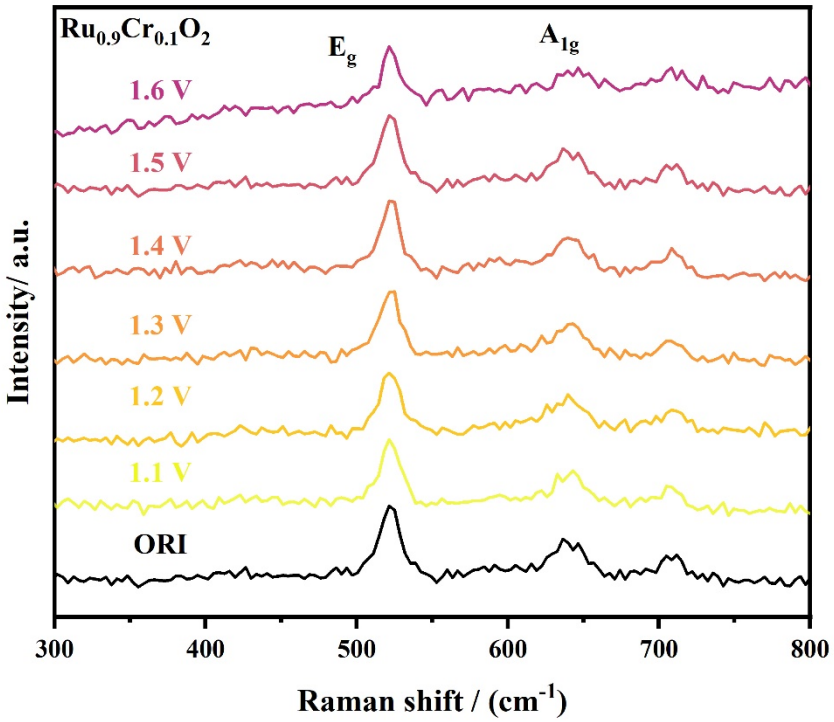

Figure S11. Operando Raman spectra obtained under various applied potential on $Ru_{0.9}Cr_{0.1}O_2$.

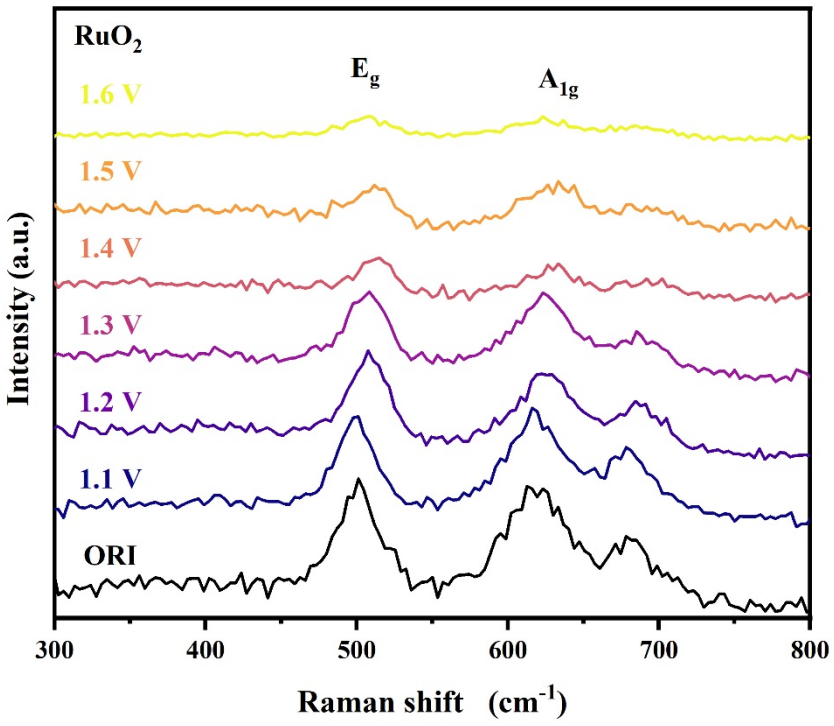

Figure S12. Operando Raman spectra obtained under various applied potential on RuO_2.

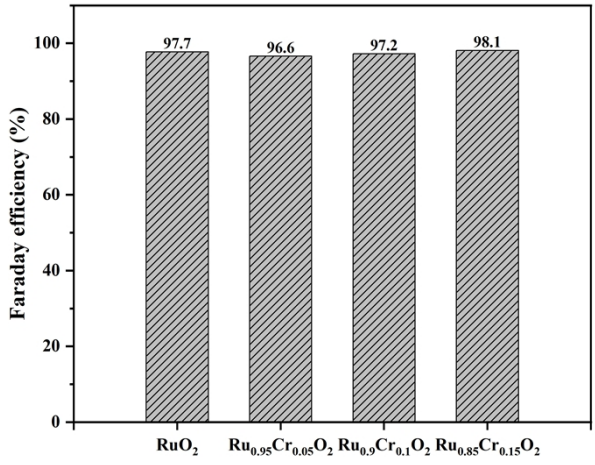

Figure S13. O_2 Faraday efficiencies of different catalysts at 10 mA cm^{-2}.

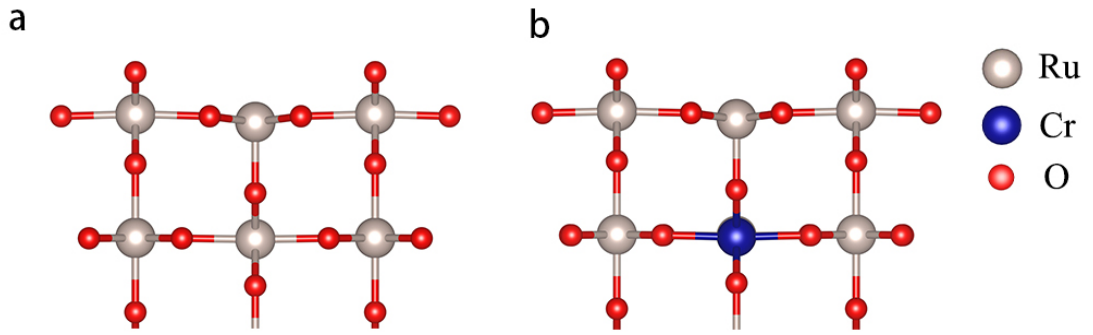

Figure S14. Model for DFT calculations of (a)RuO_2 and (b)$Ru_{0.9}Cr_{0.1}O_2$, where the grey spheres are Ru, the red ones are O and the blue ones are Cr.

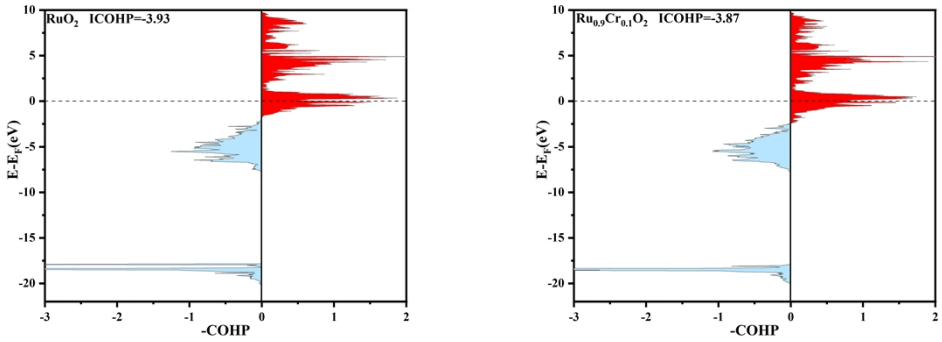

Figure S15. Description of bonding-anti-bonding roles of Ru-O bond in RuO_2 and $Ru_{0.9}Cr_{0.1}O_2$ by COHP.

Table S1. ICP-MS results of the electrolytes of RuO_2 and $Ru_{0.9}Cr_{0.1}O_2$ after a half-hour CP test.

Sample number	element	elemental concentration C（μg/L)
RuO_2	Ru	193.963
$Ru_{0.9}Cr_{0.1}O_2$	Cr	127.047
	Ru	15.683

Table S2. Formation energy of surface Ru defects in RuO_2 and $Ru_{0.9}Cr_{0.1}O_2$.

	formation energy of surface Ru defects
RuO_2	2.40 eV
$Ru_{0.9}Cr_{0.1}O_2$	2.63 eV

Table S3. d-band center of Ru PDOS and p-band center of O PDOS of RuO_2 and $Ru_{0.9}Cr_{0.1}O_2$.

	d-band center Ru PDOS	p-band center O PDOS
RuO_2	-1.085 eV	-1.237 eV
$Ru_{0.9}Cr_{0.1}O_2$	-2.726 eV	-2.975 eV